The S1-S2 linker determines the distinct pH sensitivity between ZmK2.1 and KAT1

Li Wang, Shun-Ying Yang, Man-Yuan Guo, Ya-Nan Huang, Herve Sentenac, Anne-Aliénor Véry, Yan-Hua Su

▶ **To cite this version:**

Li Wang, Shun-Ying Yang, Man-Yuan Guo, Ya-Nan Huang, Herve Sentenac, et al.. The S1-S2 linker determines the distinct pH sensitivity between ZmK2.1 and KAT1. Plant Journal, 2016, 85 (5), pp.675-685. 10.1111/tpj.13134 . hal-01595657

HAL Id: hal-01595657
https://hal.science/hal-01595657

Submitted on 26 Sep 2017

HAL is a multi-disciplinary open access archive for the deposit and dissemination of scientific research documents, whether they are published or not. The documents may come from teaching and research institutions in France or abroad, or from public or private research centers.

L'archive ouverte pluridisciplinaire **HAL**, est destinée au dépôt et à la diffusion de documents scientifiques de niveau recherche, publiés ou non, émanant des établissements d'enseignement et de recherche français ou étrangers, des laboratoires publics ou privés.

the plant journal

SEB Society for Experimental Biology

The Plant Journal (2016) **85,** 675–685 doi: 10.1111/tpj.13134

The S1–S2 linker determines the distinct pH sensitivity between ZmK2.1 and KAT1

Li Wang[1,2], Shun–Ying Yang[1], Man–Yuan Guo[1,2], Ya–Nan Huang[1,2], Hervé Sentenac[3], Anne–Aliénor Véry[3,*] and Yan–Hua Su[1]*

[1]*State Key Laboratory of Soil and Sustainable Agriculture, Institute of Soil Science, Chinese Academy of Sciences, Nanjing 210008, China,*

[2]*University of Chinese Academy of Sciences, Beijing 100049, China, and*

[3]*Biochimie & Physiologie Moléculaire des Plantes, UMR 5004, CNRS/386 INRA/SupAgro Montpellier/Université Montpellier, 34060, Montpellier Cedex 2, France*

Received 29 October 2015; revised 19 January 2016; accepted 25 January 2016; published online 5 February 2016.
*For correspondence (e-mails anne-alienor.very@supagro.inra.fr or yhsu@issas.ac.cn).

SUMMARY

Efficient stomatal opening requires activation of KAT-type K^+ channels, which mediate K^+ influx into guard cells. Most KAT-type channels are functionally facilitated by extracellular acidification. However, despite sequence and structural homologies, the maize counterpart of Arabidopsis KAT1 (ZmK2.1) is resistant to pH activation. To understand the structural determinant that results in the differential pH activation of these counterparts, we analysed chimeric channels and channels with point mutations for ZmK2.1 and its closest Arabidopsis homologue KAT1. Exchange of the S1–S2 linkers altered the pH sensitivity between the two channels, suggesting that the S1–S2 linker is essentially involved in the pH sensitivity. The effects of D92 mutation within the linker motif together with substitution of the first half of the linker largely resemble the effects of substitution of the complete linker. Topological modelling predicts that one of the two cysteines located on the outer face section of the S5 domain may serve as a potential titratable group that interacts with the S1–S2 linker. The difference between ZmK2.1 and KAT1 is predicted to be the result of the distance of the stabilized linkers from the titratable group. In KAT1, residue K85 within the linker forms a hydrogen bond with C211 that enables the pH activation; conversely, the linker of ZmK2.1 is distantly located and thus does not interact with the equivalent titration group (C208). Thus, in addition to the known structural contributors to the proton activation of KAT channels, we have uncovered a previously unidentified component that is strongly involved in this complex proton activation network.

Keywords: pH sensitivity, structural determinants, ZmK2.1, KAT1, S1–S2 linker, mutant.

INTRODUCTION

Stomatal movement is tightly regulated for the efficient uptake of CO_2 with minimal water loss. Opening of the stomatal pores requires a critical contribution of K^+ influx and accumulation into the surrounding guard cells. This process mainly, but not exclusively, relies on operation of the guard cell K_{in} channels (Schroeder *et al.*, 2001; Roelfsema and Hedrich, 2005). In Arabidopsis, the voltage-gated KAT-type channels are essential effectors of stomatal opening triggered by membrane hyperpolarization (Lebaudy *et al.*, 2008).

The plant Shaker channels, which include the KAT-type channels and the outward rectifiers of various plant species, share high degrees of structural and functional similarity (Véry and Sentenac, 2003; Véry *et al.*, 2014). This provides a fundamental basis for assessing the structural involvement in functional variation. For instance, single amino acid mutations in the SKOR channel convert this outward rectifier into an inward channel (Li *et al.*, 2008), and the pore motif is responsible for the differential voltage and pH sensitivity between AKT2/3 and KST1 (Hoth *et al.*, 2001). The activity of most KAT-type channels identified so far (e.g. KAT1, KAT2, KST1, SIRK, MIRK and AmKAT1) (Müller-Röber *et al.*, 1995; Pilot *et al.*, 2001; Pratelli *et al.*, 2002; Zhang *et al.*, 2011; Yang *et al.*, 2015) is facilitated by extracellular acidification (pH_{out}), which results in positive shifts of the activation voltages of the channels and thereby favours K^+ uptake. However, the maize counterpart of Arabidopsis KAT1 (ZmK2.1, also

© 2016 The Authors
The Plant Journal © 2016 John Wiley & Sons Ltd

known as KZM1) is insensitive to extracellular pH (Philippar *et al.*, 2003; Su *et al.*, 2005). Based on structure–function relationships demonstrated for Shaker channels, this functional difference may be attributed to their structural diversity.

Extensive evidence obtained using KAT-type channels has shown that several charged amino acid residues contribute to the KAT channel pH sensitivity (Figure 1a). Mutations of residue H118 at the cytoplasmic S2–S3 linker markedly affected the pH dependence and the activation time course of KAT1 (Tang *et al.*, 2000). At physiological pH, substitution of H118 by a negatively charged amino acid (glutamate or aspartate) slows the channel's activation time course, whereas the H118K and H118R mutations result in accelerated activation time courses. Independently of whether the substituted residue at H118 is negatively or positively charged, the mutated channels show markedly decreased sensitivity to internal pH (Tang *et al.*, 2000). For the homologue KST1 in potato (*Solanum tuberosum*), mutation of the H160 residue at the extracellular linker between the S3 and S4 segments to either positively charged (H160R), negatively charged (H160D) or neutral (H160A) amino acids generates a less pH-sensitive channel (Hoth *et al.*, 1997), suggesting a critical contribution of this amino acid to the pH regulation of KST1. In addition, the histidine (H271) at the −2 position downstream of the pore signature GYGD plays a central role in the pH modulation of KST1. Replacement of H271 leads to increased (H271D) or even inversed (H271R) pH sensitivity of KST1, and when both histidines are substituted by alanines (H160A+H271A), KST1 completely loses its pH sensitivity, suggesting that both extracellular sites are part of the pH sensor in the plant K^+ uptake channel (Hoth *et al.*, 1997). A comparative study between KAT1 and KST1 indicated that charged amino acids within the pore-forming loops contribute to, or even determine, the distinct pH sensitivity of the two channels (Hoth and Hedrich, 1999). Mutations D265N of KAT1 and D269N of KST1 both results in inverted pH sensitivity of the channels; therefore, the aspartate at this position is probably involved in pH sensing. A more recent study revealed that replacement of the negatively charged E240 of the S5–S6 linker by a neutral amino acid (E240Q) leads to partial abolishment of the acid activation effect of KAT1 (Gonzalez *et al.*, 2012). Therefore, the knowledge gained using KAT1 and KST1 strongly suggests that the pH modulation of KAT channels involves a sensory net-

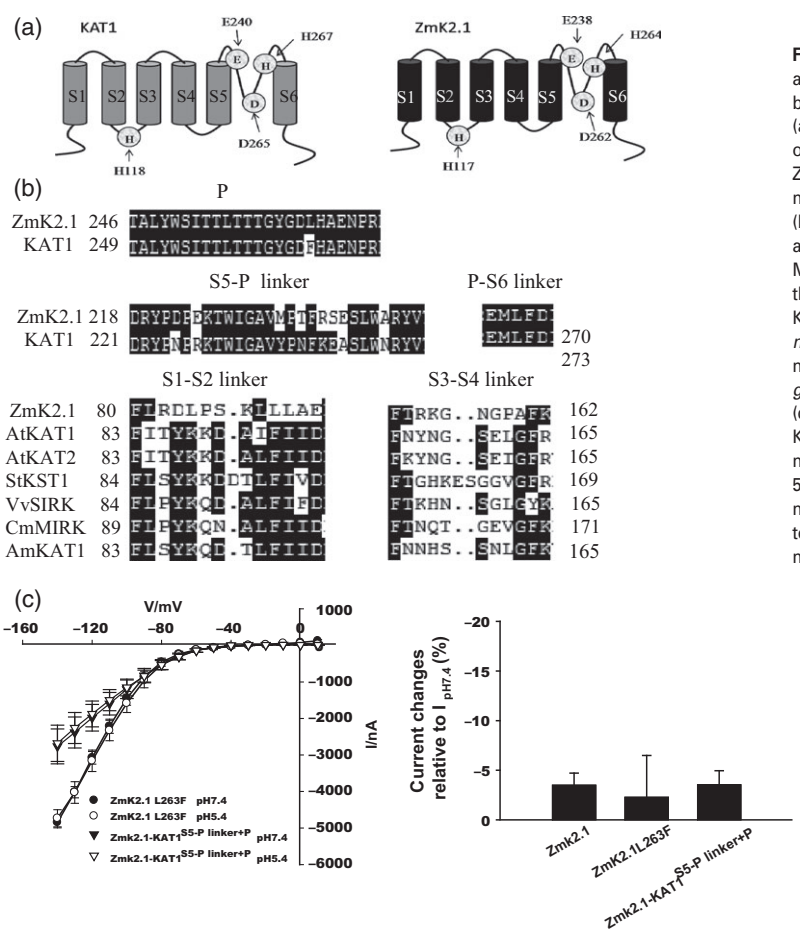

Figure 1. An unidentified structural element is predicted to account for the determination of distinct pH sensitivity between ZmK2.1 and KAT1.
(a) Amino acid residues found to contribute to pH sensitivity of the KAT1 channel (left). These residues were conserved in ZmK2.1 (right). S1–S6 represent the transmembrane segments, and P is the pore motif between segments S5 and S6.
(b) Amino acid sequence alignments between ZmK2.1, KAT1 and closely related KAT channels of various plant species. Motifs of interest are shown. The plant species from which the channels were initially identified were: Arabidopsis for KAT1 and KAT2, maize (*Zea mays*) for ZmK2.1, potato (*Solanum tuberosum*) for KST1, grapevine (*Vitis vinifera*) for SIRK, melon (*Cucumis melo*) for MIRK, and *Ammopiptanthus mongolicus* for AmKAT1.
(c) Steady-state currents for ZmK2.1 L263F and ZmK2.1–KAT1$^{S5\text{-}P\ linker\ +\ P}$ at pH 7.4 and pH 5.4, plotted against the membrane voltages (left). The bath solution contained 50 mM KCl. The bar graph (right) shows the current changes measured at −140 mV in response to a pH decrease from 7.4 to 5.4 (relative to the values at pH 7.4). Values are means ± SE (n = 3 or 4).

© 2016 The Authors

work rather than being controlled by single key amino acids. Thus, a complex proton-sensing network that is conferred by multiple charged amino acids (and probably also involves interactions among those key amino acids) accounts for the pH regulation of plant KAT channels. To obtain further insightful recognitions, it remains necessary to investigate possible mode-of-action of this network.

Beyond Shaker channels, in the animal inward rectifier HIR (the two transmembranes heart inward rectifier potassium channel), one of the two cysteines located in the M1–H5 (Cys114) and H5–M2 (Cys146) linkers serves as a potential titratable group and binds protons (Coulter *et al.*, 1995). Interaction of the histidine (H117) in the M1–H5 linker region with the titratable group (Cys114 or Cys146) leads to changes in the pore properties, and thereby determines the pH sensitivity of HIR. The pH modulation of the macroscopic current of HIR results from proton-induced changes in HIR single-channel conductance (Coulter *et al.*, 1995). These findings, as well as the related analysis, provide useful clues for identifying structural contributors to the pH sensitivity of plant KAT-type channels. Using animal Shaker channels in a comparative study of the pH-sensitive Kv1.5 channel and the pH-resistant Kv1.2 channel, Steidl and Yool (1999) demonstrated that the pH sensitivity of Kv1.5 results from an enhanced C–type inactivation at acidic pH, and that the histidine residue in the S5–P linker of Kv1.5 (H452) accounts for the difference in pH sensitivity between the Kv1.5 and Kv1.2 channels (Steidl and Yool, 1999). Single-channel recordings in lipid bilayers for individual and combined mutations of the bacterial potassium channel KcsA allowed identification of key residues (H25, E118 and E120) that are potentially protonated (Thompson *et al.*, 2008). These proton-binding sites form a complex network of inter- and intra-subunit salt bridges and hydrogen bonds near the bundle crossing (the tunnel entry that K^+ ions pass through). After a change in the proton concentration, the ionization state of the network is altered, thereby modifying the electrostatic landscape near the channel gate and influencing channel opening (Thompson *et al.*, 2008).

In addition to the conformational change in the pore due to protonation in animal and bacterial K^+ channels, the proton-induced increase in whole-cell currents for the plant inward rectifier KST1, which does not involve C–type inactivation, is due to a shift in the half-maximum activation voltage rather than an increase in single-channel conductance (Hoth *et al.*, 1997). However, a similar study established that pH activation is eventually implemented through a complex network that involves interaction of a variety of key structural elements (Gonzalez *et al.*, 2012). The amino acid sequences of ZmK2.1 and KAT1 are highly similar in terms of corresponding transmembranes and the pore motif (Su *et al.*, 2005), and the key residues involved in pH modulation identified for KAT1 are conserved in ZmK2.1 (Figure 1a,b); therefore, we assume that additional structural elements that have not been previously identified may account for their distinct pH sensitivity. To test this hypothesis, we focused on the most divergent extracellular loops: the S1–S2 and S3–S4 linkers (with <25% and 40% identity, respectively, between the two channels). We exchanged the two individual linkers between ZmK2.1 and KAT1, and observed that the S1–S2 linkers are crucially involved in determining the pH sensitivity. Furthermore, we used single-residue and combined substitutions within the S1–S2 linkers to obtain more precise details. Finally, a topology model was established to predict and interpret the mode of action of this modulatory component.

RESULTS

An additional structural element is predicted to determine the distinct pH sensitivity of ZmK2.1 and KAT1

The H118 at the internal linker between transmembranes S2 and S3 (Tang *et al.*, 2000), and E240 (Gonzalez *et al.*, 2012), D265 (Hoth and Hedrich, 1999) and H267 (Gonzalez *et al.*, 2012) of the pore motif, have been found to contribute to the pH sensitivity of KAT1 (Figure 1a, left). These residues are conserved in ZmK2.1 (Figure 1a, right). In the pore motif, ZmK2.1 and KAT1 differed by a single L/F variation (Figure 1b). Substitution of this amino acid (L263F) did not significantly influence the pH sensitivity of ZmK2.1 (Figure 1c). Based on recent studies with KAT1 indicating that certain amino acids close to the pore motif may also be involved in the proton modulation network (Gonzalez *et al.*, 2012), we tested the pore-flanking linkers (the S5–P and P–S6 linkers) for their contribution to the pH sensitivity of ZmK2.1. As the P–S6 linkers were identical between the two channels, we introduced the S5–P linker together with a pore motif from KAT1 into ZmK2.1 (ZmK2.1–KAT1$^{S5–P\ linker\ +\ P}$). The resulting chimeric ZmK2.1 channel was minimally affected by pH changes (Figure 1c), suggesting that the pore motif and pore flanking linkers do not account for the differential pH sensitivity between ZmK2.1 and KAT1. Therefore, additional structural elements were predicted to determine the distinct pH sensitivity of ZmK2.1 and KAT1. As a starting point, the extracellularly located S1–S2 and S3–S4 linkers that were highly divergent among the KAT-type channels (Figure 1b) were targeted for further assessment.

Substitution of the S1–S2 linkers reverses the pH sensitivity of ZmK2.1 and KAT1

The most divergent extracellular loops, the S1–S2 and S3–S4 linkers, were exchanged between ZmK2.1 and KAT1 to generate two pairs of chimeric channels, namely ZmK2.1–Δ1 and KAT1–Δ1 plus ZmK2.1–Δ2 and KAT1–Δ2 (Figure 2a,b).

© 2016 The Authors

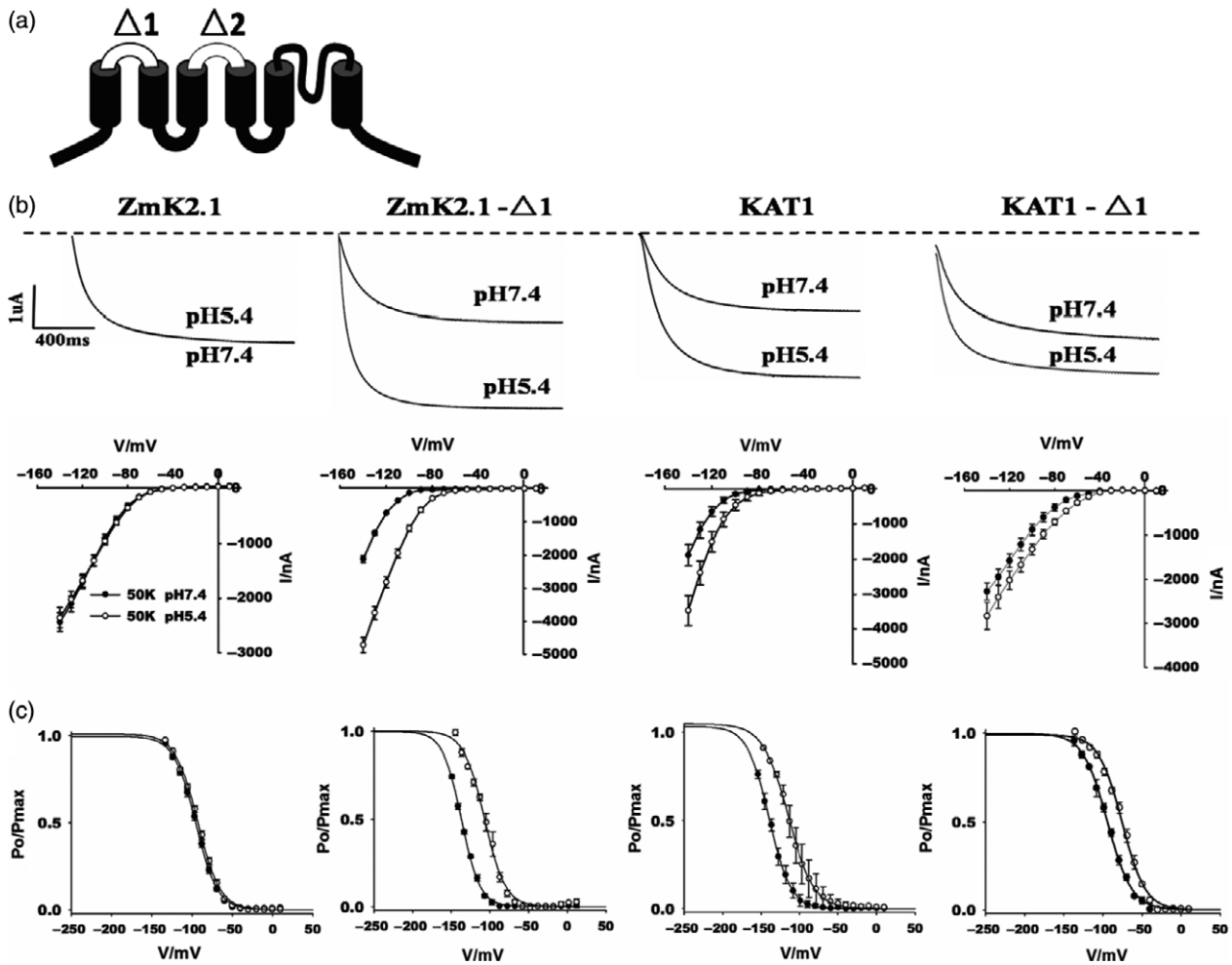

Figure 2. Substitution of the S1–S2 linkers reverses the pH sensitivity between ZmK2.1 and KAT1.
(a) A schematic drawing indicates substitutions made between ZmK2.1 and KAT1. Δ1, replacement of the S1–S2 linkers; Δ2, substitutions between the S3–S4 linkers.
(b) Representative current traces recorded in response to voltage pulses of −140 mV for oocytes expressing ZmK2.1, ZmK2.1–Δ1, KAT1 or KAT1–Δ1 in response to 50 mM K^+ at pH 7.4 or 5.4 (upper panels). The traces were superimposed. Steady-state currents for ZmK2.1, ZmK2.1–Δ1, KAT1 and KAT1–Δ1, plotted against the membrane voltages at pH 7.4 or pH 5.4 (lower panels).
(c) Effects of pH on channels gating at pH 7.4 (closed circles) and pH 5.4 (open circles). Deactivation tail currents were measured at –40mV after voltage pulses ranging from –140 to 10mV with 10mV increment (see the Figure S1), and are expressed relative to the deduced values at which maximal opening probability was achieved. The solid lines represent Boltzmann fits to the data. The half-maximal activation voltages ($V_{½}$) were −95.4 ± 0.7 mV for ZmK2.1 at pH 7.4, −92.9 ± 0.8 mV for ZmK2.1 at pH 5.4, −137 ± 1.6 mV for ZmK2.1–Δ1 at pH 7.4, −107 ± 1.5 mV for ZmK2.1–Δ1 at pH 5.4, −139.9 ± 1.2 mV for KAT1 at pH 7.4, −114.7 ± 1 mV for KAT1 at pH 5.4, −94 ± 0.9 mV for KAT1–Δ1 at pH 7.4, and −75.3 ± 1.1 mV for KAT1–Δ1 at pH 5.4. Values are means ± SE (n = 4–7).

The electrophysiological properties of the chimeras were investigated using two-electrode voltage clamping in the *Xenopus* oocyte expression system.

Consistent with previous reports, the macroscopic current of ZmK2.1 was little affected following a decrease in pH from 7.4 to 5.4 (Figure 2b) (Philippar *et al.*, 2003; Su *et al.*, 2005). In contrast, KAT1 activity was markedly induced by the acidic pH, resulting in a current increase of 89.8 ± 9.6% at −140 mV in response to a two-unit decrease in external pH (Figure 2b) (Véry *et al.*, 1995; Hoth and Hedrich, 1999). Substitution of the S1–S2 linker with the matching part from KAT1 essentially converted ZmK2.1 into an acid activated channel (125.5 ± 18.1% current increase at −140 mV as the pH decreased from 7.4 to 5.4), resembling the magnitude of the pH modulation of KAT1 (ZmK2.1–Δ1, Figure 2b). In addition, the reciprocal substitution dramatically decreased the pH sensitivity of KAT1, with an acid-induced current increase of only approximately 24.2 ± 6.5%, as measured at −140 mV (KAT1–Δ1, Figure 2b). As described elsewhere (Hoth *et al.*, 1997), such acid activation resulted in positive shifts of the half-maximal activation voltages of 33 ± 3.3, 27.3 ± 4.3 and 19.5 ± 1.5 mV for ZmK2.1–Δ1, KAT1 and KAT1–Δ1, respectively (Figure 2c). In contrast, the half-maximal activation

© 2016 The Authors

voltage of ZmK2.1 remained almost unchanged ($\Delta V_{½}$ was approximately 3.0 ± 1.3 mV when shifting the pH from 7.4 to 5.4 , Figure 2c). Taken together, these observations suggest a crucial role of the S1–S2 linker in determining the distinct pH sensitivity between the ZmK2.1 and KAT1 channels. Such acid activation is in line with the positive shifts of the half-maximal activation voltages that favoured the operation of the channels.

The S1–S2 linker also influences the activation and deactivation kinetics of ZmK2.1 and KAT1

In line with previous reports (Véry *et al.*, 1995; Su *et al.*, 2005), ZmK2.1 showed a mode of action comprising faster activation/slower deactivation, whereas that for KAT1 was the opposite (Figure 3a). At pH 7.4, the half-maximal activation time ($t_{½}$) of ZmK2.1 was 69.8 ± 3.2 msec, approximately half of that of KAT1 (161.6 ± 10.5 msec, Figure 3a). Conversely, the half-deactivation times ($t_{d½}$) determined for ZmK2.1 and KAT1 were 43.7 ± 3.2 and 33.1 ± 7.3 msec, respectively (Figure 3a,b). At acidic pH 5.4, the activation of KAT1 was accelerated ($t_{½}$ = 119.4 ± 10.5 msec), but its deactivation slowed down ($t_{d½}$ = 43.5 ± 7.4 msec). However, the activation of ZmK2.1 was almost unaffected ($t_{½}$ = 73.6 ± 3.1 msec). Exchange of the S1–S2 linkers reversed the activation/deactivation kinetics of the chimeric channels (ZmK2.1–Δ1 and KAT1–Δ1) to a certain extent (Figure 3a,b). These results suggest that the S1–S2 linkers may also be involved in shaping the time courses of channel activation and deactivation between the two channels. However, it remains to be clarified whether an intrinsic link exists between the pH sensitivity and the activation time course of the channel effected by the S1–S2 Linker.

Unlike substitution of the S1–S2 linkers, exchange of the S3–S4 linkers between ZmK2.1 and KAT1 did not result in significant changes of gating properties at pH 7.4 when compared to the wild-type channel. (ZmK2.1–Δ2 $V_{½}$ = 94.2 ± 2.7 mV versus ZmK2.1 $V_{½}$ = 96.4 ± 1.5 mV; KAT1–Δ2 $V_{½}$ = −133.1 ± 3.2 mV versus KAT1 $V_{½}$ =

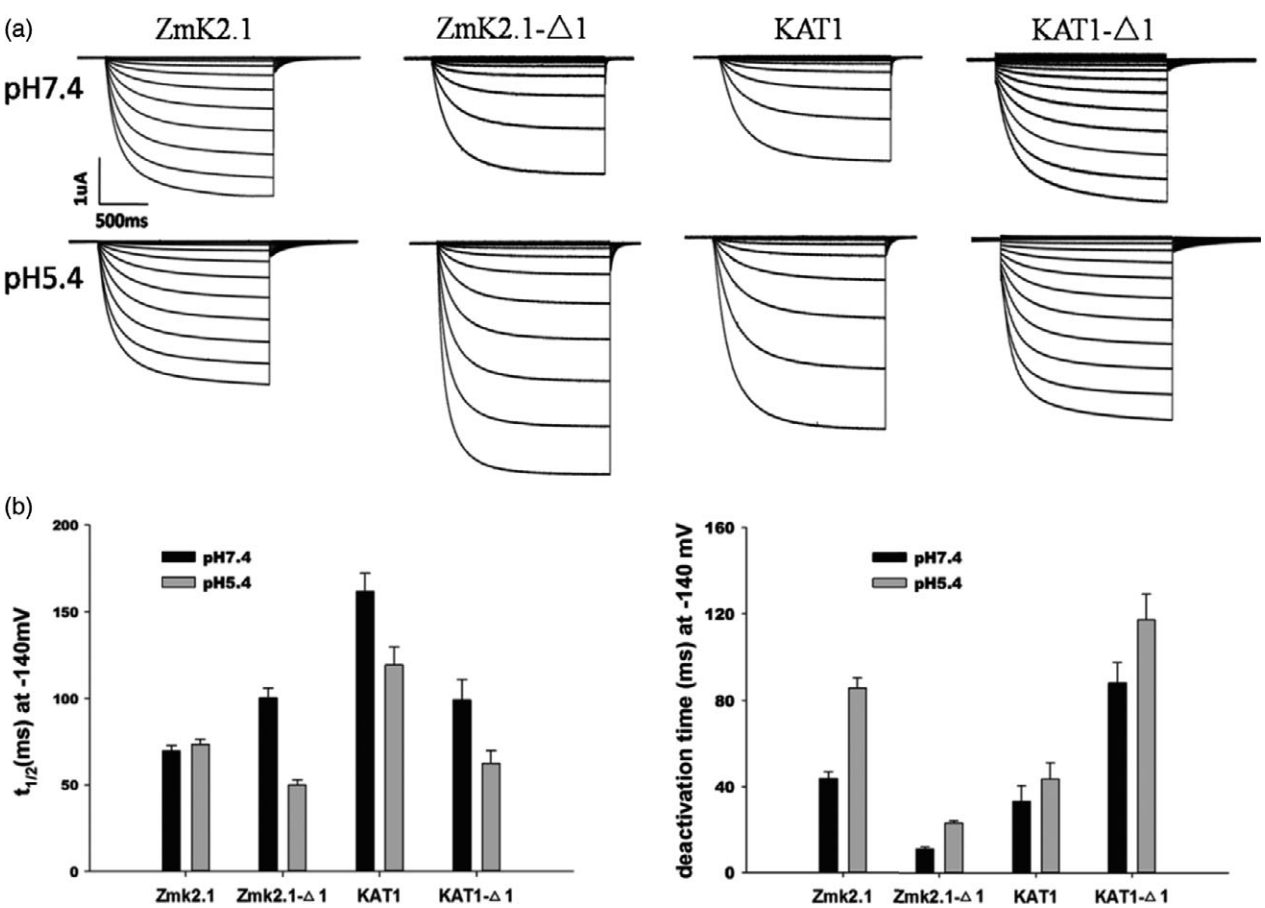

Figure 3. The S1–S2 linkers are involved in determining the activation and deactivation kinetics.
(a) Representative current traces for ZmK2.1, ZmK2.1–Δ1, KAT1 and KAT1–Δ1 recorded in 50 mM external K^+ solutions at pH 7.4 or pH 5.4. In all recordings, the holding potential was −40 mV, and voltage pulses range from –140 to 10 mV with 10 mV increments for a duration of 1.5 sec.
(b) Half-activation ($t_{1/2}$) and deactivation time constant ($t_{d1/2}$ of wild-type and chimeric channels and changes in response to external pH. $t_{1/2}$ was evaluated as the time to reach half of the steady current amplitude at 1.5 sec in response to a voltage pulse −140 mV from a holding potential of −40 mV. The $t_{d½}$ is the time constant for half-deactivation of the tail current at −140 mV, as obtained by fitting the tail currents with single exponential (recorded on return to the holding potential). Values are means ± SE (n = 4–6).

© 2016 The Authors

−137.9 ± 3.7 mV). At acidic pH (5.4), substitution of the S3–S4 linker (ZmK2.1–Δ2) resulted in significant leak currents (Figure S2a), implying drastic alteration of the channel's voltage dependence and rectification. This change, although accompanied by an effect on pH modulation, may have rather confusing effects beyond the influence on the pH sensitivity. Moreover, the opposite substitution resulted in a reduction of only approximately 27% in the acid-activated current amplitude of ZmK2.1 –Δ2 (containing the S3–S4 linker of KAT1, Figure S2b: 89.8 ± 9.6% and 66.1 ± 6.8% of the acid-induced current increase for the wildtype KAT1 and KAT1–Δ2, respectively). Therefore, the S3–S4 linker shows multiple effects on the channel and only partly contributes to the pH sensitivity of ZmK2.1 and KAT1, and thus was excluded from further assessment.

Individual amino acid substitutions within the S1–S2 linker are not sufficient to confer the differences in pH regulation

The results of the above experiments support a vital role for the S1–S2 linker in controlling the extracellular pH regulation between ZmK2.1 and KAT1. To obtain further insight into the key determinants of such modulation, we generated single amino acid mutations within the S1–S2 linker of ZmK2.1 based on alignment with the equivalent sites in KAT1 (Figure 4a). The resulting single-site mutated proteins were then assessed for their effect on the magnitudes of the acid-activated currents. Surprisingly, substitution of the aspartic acid residue at position 83 by a tyrosine (D83Y) resulted in no detectable current for ZmK2.1, and this mutant was therefore excluded from further analysis. At 50 mM extracellular K^+, the P85K mutation (corresponding to position 88 in KAT1) was elicited largely reduced k^+ current (Figure 4b). The current amplitudes of the remaining single-site mutated channels were variably affected but not dramatically changed. Changes in the pH_{out} sensitivity of mutants with single amino acid substitutions were further evaluated in terms of the percentage current increase at −140 mV in response to a pH decrease from 7.4 to 5.4 compared to the currents of the wild-type ZmK2.1 channel and the chimera ZmK2.1–Δ1 (Figure 4c). With respect to the wild-type channel, S86D, K87A and E92D substitutions resulted in slight increases in acid-induced current amplitudes (6.0 ± 1.5%, 6.9 ± 1% and 8.7 ± 1.4%, respectively), and the P85K mutation conferred an acid-induced change of approximately 16.4 ± 4.1% (Figure 4b,c). However, these changes in the pH sensitivity were much lower than the 125% increase in acid-activated current achieved with ZmK2.1–Δ1 (Figure 4c). Similarly, the L81I, R82T, L84K, L88I or L89F single-site mutations did not result in clearly measurable proton activation (Figure 4c). Substitutions at positions 90 or 91 (L90I and A91I) resulted in reductions in current of approximately 23% as a result of acidification (Figure 4b,c). However, such effects accounted for less than one-fifth of the acid-modulated current increase observed for ZmK2.1–Δ1, in the opposite direction. Hence, these results demonstrate that single-site substitutions within the S1–S2 linker of ZmK2.1 were not sufficient to replicate the remarkably effective proton activation conferred by replacement of the the whole linker (ZmK2.1–Δ1).

Combined substitution of E92D and the upstream half loop has an effect on proton activation equivalent to replacement of the entire S1–S2 linker

Because individual amino acid substitutions do not effectively alter the pH sensitivity of ZmK2.1, we speculated that mutations of combinations of amino acids in a continuous sequence within the S1–S2 linker may produce a notable modification to the pH sensitivity of ZmK2.1. To test this hypothesis, we divided the S1–S2 linker of ZmK2.1 into two parts, namely Q (positions 80–87) and H (positions 88–92) (Figure 4a), which were replaced by the equivalent sections from KAT1 to obtain chimeric channels ZmK2.1–ΔQ and ZmK2.1–ΔH. After expression in oocytes, the ZmK2.1–ΔQ and ZmK2.1–ΔH chimeras showed 48.7 ± 11.1% and 50.9 ± 5.1% macroscopic current increases, respectively, measured at −140 mV, upon acidification from pH 7.4 to 5.4 (Figure 5a,c). Additively, these effects were comparable to the increase in proton-activated current for KAT1 (89.8 ± 9.6%), and similar to the proton-activated effects of ZmK2.1–Δ1 (125.5 ± 18.1%, Figure 5c). Moreover, as expected, the half-activation voltages of the ZmK2.1–ΔQ and ZmK2.1–ΔH chimeras were shifted by 16.8 ± 0.7 mV and 19.8 ± 3.3 mV, respectively, towards less hyperpolarized directions (Figure 5b). This finding suggests that the Q and H sub-domains are additively required for controlling the pH sensitivity of ZmK2.1.

The charged amino acids are the most likely targeting sites of the proton action network (Hoth *et al.*, 1997; Hoth and Hedrich, 1999; Gonzalez *et al.*, 2012), the Q sub-domains between ZmK2.1 and KAT1 showed more divergence with respect to charged residues (Figure 5a), while the H sub-domains of the counterparts were equally negatively charged (E92 in ZmK2.1 and D95 in KAT1, respectively, see Figure 4a). Moreover, the Q and H sub-domains almost equally contributed to the pH sensitivity of ZmK2.1 and KAT1. Therefore, we tested the combined substitution/mutation ZmK2.1–ΔQ + E92D (Q from KAT1, and E92 mutated to D as in KAT1, see Figure 5a). As shown in Figure 5(a,c), ZmK2.1–ΔQ + E92D showed enhancement of the acid-activation effect of KAT1, resembling that of ZmK2.1–Δ1. The half-activation voltage of ZmK2.1–ΔQ + E92D positively shifted to 30.4 ± 3.8 mV upon a pH decrease from 7.4 to 5.4 (Figure 5b), and was accompanied by a macroscopic current amplitude increase of 106.1 ± 21.9%. These properties are consistent with the results for KAT1 and ZmK2.1–Δ1 (Figure 5c; compare with Figure 2b). Conversely, the substitution KAT1–ΔQ + D95E (Q from ZmK2.1,

© 2016 The Authors

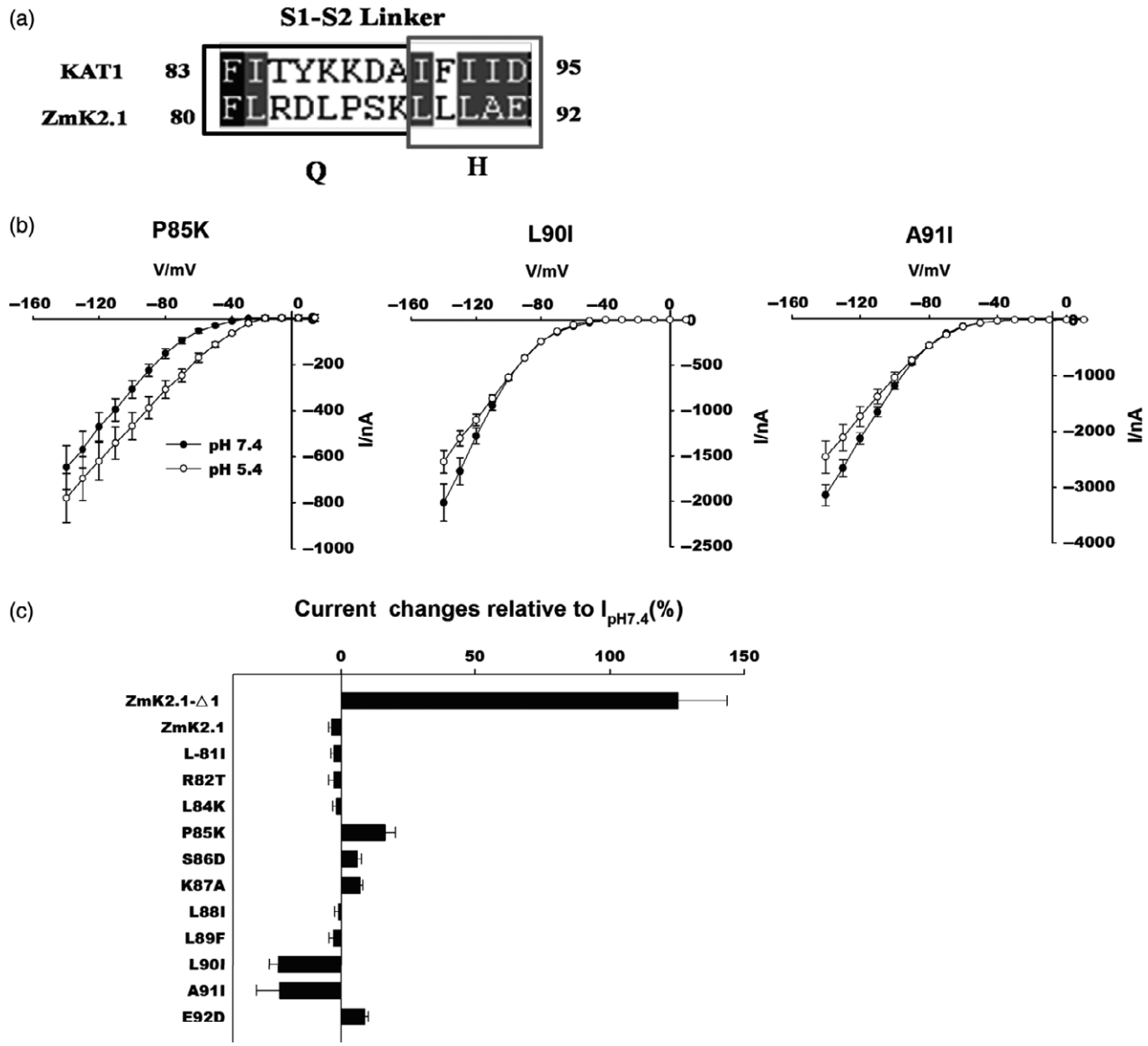

Figure 4. Individual amino acid substitutions within the S1–S2 linker are not sufficient to alter the pH sensitivity.
(a) Alignment of ZmK2.1 and KAT1 amino acid sequences within the S1–S2 linker. Individual amino acids of ZmK2.1 were mutated to the residues present in KAT1. For half-domain and combined substitutions, the linker was divided into two sub-domains: Q (positions 80–87) and H (positions 88–92).
(b) The current–voltage relationship of point mutations P85K, L90I and A91I with >10% changes in pH effects relative to the wild-type ZmK2.1. The mutation P85K resulted in approximately 16.4 ± 4.1% of the acid-induced effect of the proton activated current increase, and L90I and A91I showed approximately 23% of the inhibitory effect upon external acidification from pH 7.4 to pH 5.4. The measuring conditions were 50 mM external K^+ at pH 7.4 or pH 5.4. Error bars represent variations from at least three individual oocytes.
(c) The pH effects of point mutations are expressed as percentage current changes relative to the current measured at pH 7.4, pH effect = $(I_{pH5.4} - I_{pH7.4})/I_{pH7.4} \times 100\%$. Values were measured at −140 mV with 50 mM external K^+ in the bath solutions. Values are means ± SE of at least three oocytes.

and D95 mutated to E as in ZmK2.1), decreased the pH activation of the resulting channel to approximately 21.8 ± 4.9% (n = 4, Figure 5c, right). These results resembled those for the whole S1–S2 linker substitution (KAT1–Δ1, 24.2 ± 6.5%, Figure 2). Therefore, the moietie Q and D/E residue at position 95 ultimately determine the pH sensitivity between ZmK2.1 and AtKAT1. Accompanied by the pH effects on the current amplitude, we observed a 15.8 ± 2.5 mV positive shift of the half-activation voltage. Thus, we confirmed the pivotal role of the S1–S2 linker, specifically the Q sub-loop together with residue E92, in determining the pH sensitivity between ZmK2.1 and KAT1.

Modelling interpretation of the S1–S2 linker as a novel component in the proton modulation network

A topology model was created using crystallized KvAP from *Aeropyrum pernix* (Jiang *et al.*, 2003) as the best matching template to interpret the possible mode of action

© 2016 The Authors

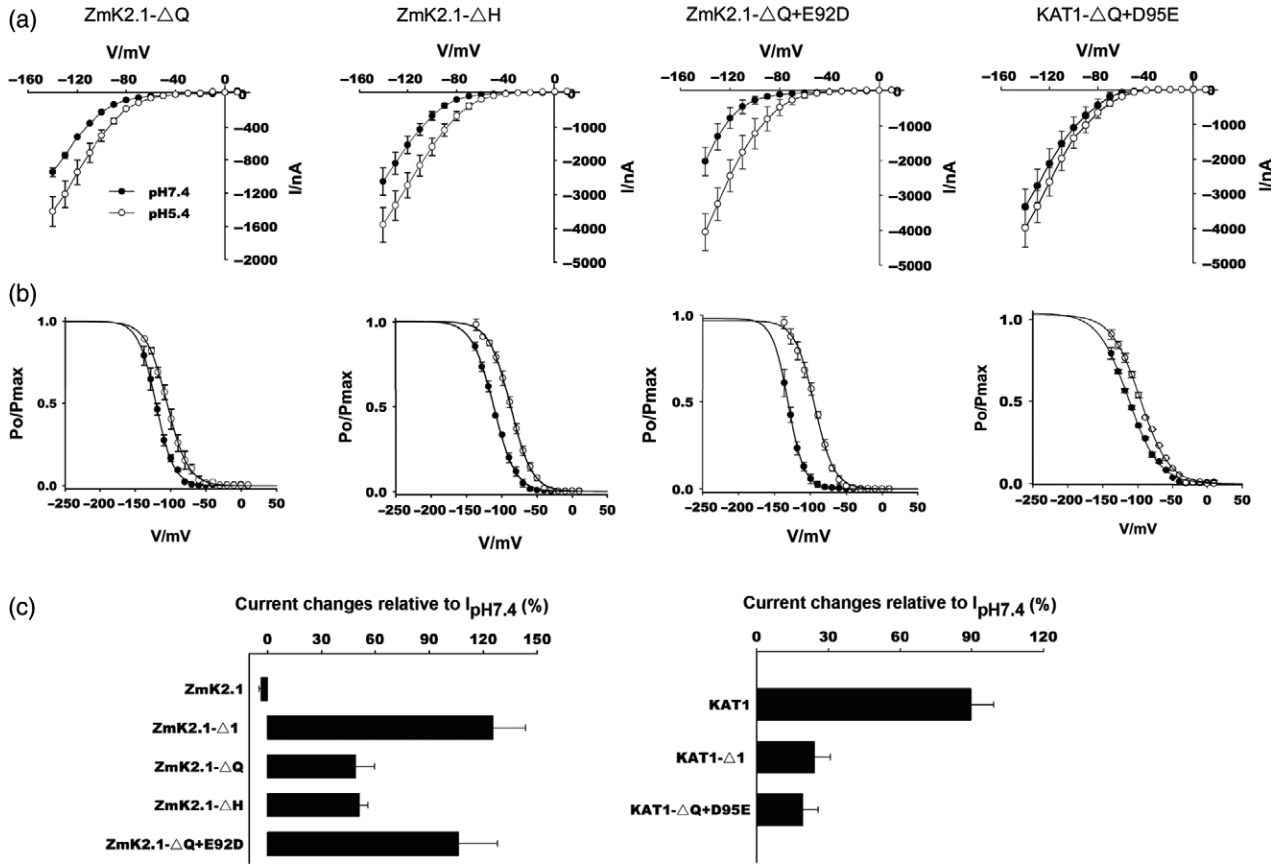

Figure 5. The two halves of the S1–S2 linker are additively responsible for the changes in pH modulation.
(a) Current–voltage relationships of ZmK2.1–ΔQ, ZmK2.1–ΔH, ZmK2.1–ΔQ + E92D and KAT1–ΔQ + D95E at pH 7.4 or pH 5.4. The bath solutions contained 50 mM external K^+.
(b) Changes in gating properties of the chimeric channels. Deactivation tail currents were measured at –40 mV after voltage pulses ranging from –140 mV to 10 mV with 10 mV increment, and are expressed relative to the deduced values at which maximal opening is achieved. Closed circles represent values at pH 7.4; open circles represent values at pH 5.4. The external solution contained 50 mM K^+. The following half-maximal activation voltages ($V_{½}$) were obtained from Boltzmann fits to the data (solid lines): ZmK2.1– ΔQ, $V_{½} = -120.8 \pm 2.5$ mV at pH 7.4 and -105.0 ± 2.9 mV at pH 5.4; ZmK2.1 –ΔH, $V_{½} = -106.9 \pm 1.6$ mV at pH 7.4 and -107 ± 1.5 mV at pH 5.4; ZmK2.1– ΔQ + E92D, $V_{½} = -130.1 \pm 3.5$ mV at pH 7.4 and -100.1 ± 8.0 mV at pH 5.4; KAT1– ΔQ + D95E, $V_{½} = -114.5 \pm 2.1$ mV at pH 7.4 and -98.8 ± 1.8 mV at pH 5.4.
(c) pH effects of combination mutations expressed as percentage current changes relative to the current measured at pH 7.4 $[(I_{pH5.4} - I_{pH7.4})/I_{pH7.4} \times 100\%]$, compared with the wild-type channels. Values were measured at −140 mV with 50 mM external K^+ in the bath solutions. Values are means ± SE of at least three oocytes.

of the S1–S2 linker within the framework of the proton modulation network (Figure 6). The cysteine (C208) located in the extracellular section of S5 was predicted to act as a potential titratable group (Coulter *et al.*, 1995), and the position changes of P85 or K85 in the highly flexible S1–S2 linker were deduced to represent modifications to the electrostatic- or bond- interactions between the linker and the titratable C208. In wild-type ZmK2.1, the S1–S2 linker is distantly located from C208 (Figure 6, P85(WT), green). When replaced by the KAT1 linker (MUTA-1 = ZmK2.1–Δ1, cyan) or its functional equivalent MUTA–2 (ZmK2.1–ΔQ + E92D, magenta), hydrogen-bond interactions between K85 and C208 were observed (2.7 Å for MUTA–1 and 3.1 Å for MUTA–2). This finding indicates that, due to interactions with the potential titratable group, the S1–S2 linkers determine the pH sensitivity between ZmK2.1 and KAT1. Therefore, in addition to the current recognitions that many single site amino acid residues contribute to the pH sensitivity of KAT type channels, this linker probably represents another critical, and domain-wised component that acts within the proton activation network. To test this hypothesis, we mutated C208 in the background of ZmK2.1–ΔQ + E92D (a mutant that greatly resembles AtKAT1), substituting the Cys residue by the non-titratable residues Gly, Ala or Asp. As shown in Figure S3b, and similar to the findings with the animal heart inward rectifier HIR (Coulter *et al.*, 1995), changes to C208 resulted in drastic reductions of the channel currents to less than 25% of macroscopic current amplitudes (within −200 to −300 nA when measured at −140 mV, pH 7.4, n => 6–8). The C208D mutant did not show a detectable current in oocytes. For the C208G or C208A substitutions, when evaluated with the resulting small currents (although this may lead to less convincing estimations), the pH activation effects were

© 2016 The Authors

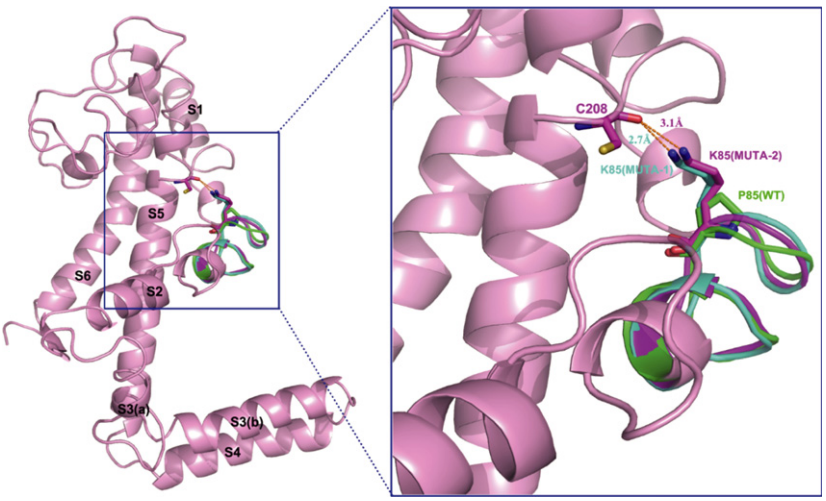

Figure 6. Topology modeling of possible interactions between the S1–S2 linker and the potential titratable group.
A topology model of the wild-type ZmK2.1 channel was constructed by homology modeling to the crystal structure of the KvAP K^+ channel (Jiang *et al.*, 2003) using an approach similar to that previously described (Yang *et al.*, 2015). For dynamic predictions, we focused on the S1–S2 linker of ZmK2.1 and its KAT1 substitutions (MUTA–1: ZmK2.1–Δ1; MUTA–2: ZmK2.1–ΔQ + E92D). The various configurations of the S1–S2 linker are shown: WT, green; MUTA–1, cyan; MUTA–2, magenta. In MUTA–1 and MUTA–2, the potential titratable group, C208, was predicted to form hydrogen bond interactions with K85, which showed positions close to its initial position in KAT1: K85 was predicted to be located 2.7 Å from C208 in MUTA-1, and 3.1 Å from C208 in MUTA-2.

only approximately 30% of that of ZmK2.1–ΔQ + E92D (Figure S3b). These data indicate that C208 is important for channel function and pH activation.

Because C211 in the S5 segment is located close to C208, we also tested a C211A mutant. Similar to the mutations to C208, C211A resulted in a reduction of the current of approximately 75%. Thus, both cysteine residues appear to be important for the function of ZmK2.1 and ZmK2.1–ΔQ + E92D. Based on interaction predictions between individual residues (S1–S2 linker versus S5–P region), within the framework of our model, only K85 (P85 in ZmK2.1 WT) is able to form a stabilized hydrogen-bond interaction with C208. C211 is located beyond the range for stable interactions with residues of the S1–S2 linker. Furthermore, the C211A mutant, although associated with a markedly reduced current amplitude, retained 63 ± 7% (n = 4) of the pH activation effect (Figure S3). Therefore, based on the modelling predictions and similar experimental observations to those described for HIR (Coulter *et al.*, 1995), we hypothesize that C208 may play a central role in interacting with the S1–S2 linker.

DISCUSSION

In contrast to most KAT-type channels identified so far, including the best assessed channel Arabidopsis KAT1, ZmK2.1 has two particular functional properties, namely dependence on the presence of an external K^+ for channel activation, and lack of activation by extracellular acidification (Su *et al.*, 2005). However, the amino acids of the transmembranes are highly similar to those of KAT1, with an overall identity of 88%. The channels share almost identical amino acid sequences within the pore-forming motif (P), with only an L/F substitution at the −1 position downstream of the GYGD signature. In the voltage sensor domain (S4), ZmK2.1 and KAT1 are similarly positively charged (seven positively charged amino acid residues and two negatively charged amino acid residues at equivalent positions), and ZmK2.1 shows N/S and H/R substitutions relative to KAT1 (Su *et al.*, 2005). Thus, these channels provide an excellent paired model for addressing the structural basis of functional diversity. Using this model, we resolved the molecular determinants of the distinct pH sensitivity of the counterparts.

Our results show that one of the most divergent extracellular loops, the S1–S2 linker, is largely responsible for determining the pH regulation between ZmK2.1 and KAT1. Reciprocal substitution of the linker generally results in exchange of pH sensitivity between the two channels (Figure 2b), suggesting a major contribution of the S1–S2 linker to pH modulation. However, it should be noted that, although KAT1 substituted with the 'suppressive' S1–S2 linker from ZmK2.1 is much less pH sensitive, the channel retains approximately 24% of pH-activated current amplitude (Figure 2b). This finding suggests that multiple structural contributors act within the network (Gonzalez *et al.*, 2012). The present work also shows that proton activation of the KAT channels is favoured by a positive shift of the channel's activation voltage to less hyperpolarized membrane potentials ($V_{½}$ shifts; see also Figure 2c) (Müller-Röber *et al.*,1995; Pilot *et al.*, 2001; Pratelli *et al.*, 2002; Zhang *et al.*, 2011). The dynamics of the open probability are laterally shifted without significant changes in steepness (Figures 2c and 5b), consistent with the previous finding that the single-channel conductance of KST1 was little affected upon acid activation of the channel (Hoth *et al.*, 1997), and may differ from the results for animal K^+ channels that extracellular proton often result in changes in channel conductance (Coulter *et al.*, 1995; Steidl and Yool, 1999; Thompson *et al.*, 2008).

Associated with the changes in macroscopic current amplitudes is the influence of the S1–S2 linker on the activation/deactivation kinetics of the channels (Figure 3a,b). Extracellular acidification accelerates the activation of KAT1, and, consistent with its resistance to pH modulation, the acti-

© 2016 The Authors

vation of ZmK2.1 remains almost unaffected, suggesting a correlation between activation of the channels and their sensitivity to protons. In accordance with the macroscopic transition, exchange of the S1–S2 linkers converts ZmK2.1 and KAT1 to show the activation and deactivation kinetics of their counterparts (Figure 3a,b), suggesting that the S1–S2 linkers play a role in fine tuning of the time courses of activation and deactivation of the channels.

Further individual and combined substitutions within the S1–S2 linker suggest that E92 together with the first half of the loop replace the role of the intact linker (Figure 5c). This observation also implies that, in addition to interactions among key individual contributors (Gonzalez *et al.*, 2012), the involvement of a motif-wised structural component may also exist.

Based on experiments with animal and bacterial K^+ channels, proton modulation involves interactions between a protonation residue and titratable or proton-binding sites that form a proton modulation network (Coulter *et al.*, 1995; Steidl and Yool, 1999; Thompson *et al.*, 2008). To identify and interpret the mode of action of the S1–S2 linker within the modulation network, ZmK2.1 was subjected to homologous modelling with KvAP as the best matching template (Jiang *et al.*, 2003). Through amino acid sequence analysis and predictions using the topology model, C208 at the outer face was identified as a potentially titratable group (Figure 6). The linker of ZmK2.1 is predicted to be distant from the C208, and thus has a lower probability of interacting with C208. In contrast, the linker of KAT1 may form a hydrogen bond with the titratable group (Figure 6). This observation accounts for the differences in pH modulation between ZmK2.1 and KAT1.

Furthermore, among the KAT-type channels, the amino acid sequences spanning the S5–P segments contain only two cysteine residues, but these are strictly conserved (equivalent to C208 and C211 here, Figure S3a), possibly implying a common role and/or mode of action of C208. However, confirmation of this speculation requires further experimentation using homologues from other species, such as KST1, VvSIRK and AmKAT1.

In conclusion, the S1–S2 linker may represent a structural element that acts in the proton modulation network and determines the pH sensitivity of ZmK2.1 and KAT1, possibly via differential interaction with the titratable group. This mechanism may be conserved among plant KAT-type channels.

EXPERIMENTAL PROCEDURES

Molecular biology

Chimeras between ZmK2.1 and KAT1 and point mutants were generated using the overlapping PCR method (Yon and Fried, 1989). PCR amplification was performed with PrimerSTAR HS DNA polymerase (TaKaRa, http://www.takara-bio.com) according to the manufacturer's instructions. PCR products were cloned into the pMD19-T vector [Takara Biotechnology (Dalian) Co. Ltd., http://www.takara.com.cn], and the accuracy of the desired mutation was verified by sequencing. For expression, the chimeric channels and mutants were cloned into the mammalian expression vector pCI (Promega, http://www.promega.com) between the *Xba*I and *Not*I sites.

Oocyte preparation

Oocytes were obtained from anesthetized mature female *Xenopus laevis* frogs, and treated with 1 mg ml^{-1} collagenase A (Roche, http://www.roche.com) for approximately 2 h in Ca^{2+}-free medium containing 82.5 mM NaCl, 2 mM KCl, 1 mM $MgCl_2$ and 5 mM HEPES pH 7.4. Stage V and VI oocytes were selected and placed in ND96 medium containing 96 mM NaCl, 2 mM KCl, 1.8 mM $CaCl_2$, 1 mM $MgCl_2$ and 5 mM HEPES pH 7.4, supplemented with 50 mg L^{-1} gentamicin. Experimental oocytes were micro-injected using a Nanoliter 2000 microinjection system World Precision Instruments, http://www.wpiinc.cn with 59.8 nl plasmid DNA and control oocytes were injected with 59.8 nl deionized water, and oocytes were then incubated in ND96 medium for 2–3 days at 20°C for gene expression.

Electrophysiological recordings

Whole-oocyte recordings were performed using an Axoclamp 900A two-electrode voltage clamp amplifier (Axon Instruments, Molecular Devices, http://www.moleculardevices.com), Glass microelectrodes (approximately 1.5 MΩ) were filled with 3 M KCl. Data were sampled at 10 kHz, low-pass filtered at 2 kHz, and digitized using a Digidata 1440A digitizer (Axon Instruments, Molecular Devices). Measurements were performed in bath solutions containing 50 mM KCl, 50 mM NaCl, 1 mM $MgCl_2$, 1.8 mM $CaCl_2$, buffered with 5 mM HEPES (pH 7.4) and 5 mM MES (pH 5.4). For measurement of the pH effects, currents were initially measured at 50 mM K^+ (pH 7.4), and then measured at 50 mM K^+ (pH 5.4). Finallly the solution (50 mM K^+, pH 7.4) was re-applied to the bath after the pH 5.4 test, which make sure that the changes in current amplitudes observed during the experiment were indeed due the effect of pH rather than extraneous factors. Recordings were performed at 20–22°C.

Data analysis

Current traces and *I*/*V* relationships were first analysed using Clampfit version 10 (Molecular Devices), and graphs and statistics were finalized using SigmaPlot software (Systat Software, http://www.sigmaplot.com). Tail currents were recorded at a holding potential of −40 mV after a series of hyper- and de-polarizing voltage pulses. P_o/P_{max} was calculated by fitting the tail-current amplitude/membrane potential curve with a simple Boltzmann equation, using the following function: $P_o/P_{max} = [1/Z_g\ (1 + \exp((V - V_{½})\ F/RT)]$, where R, T and F represent ideal gas constant, absolute temperature and Faraday's constant, respectively, Z_g represents the number of equivalent charges, and $V_{½}$ is the half-activation voltage, at which 50% of the maximum opening of the pore is reached. The $t_{1/2}$ was evaluated as the time to reach the half of the steady current amplitude at a voltage pulse –140 mV and $t_{d½}$ is the time constant for half-deactivation of the tail current at −140 mV, as obtained by fitting the tail currents with a single exponential (recorded on return to the holding potential). Unless otherwise mentioned, the results are means ± SE from at least three individual oocytes (Figure S1).

Homology modelling

The target sequences of wild-type ZmK2.1 (WT), MUTA–1 and MUTA–2 were selected as the input for homology modelling. The

© 2016 The Authors

crystal structure of KvAP from *Aeropyrum pernix* (PDB ID 1ORQ) (Jiang *et al*., 2003) was downloaded from the Protein Data Bank (Berman *et al*., 2000) for use as the template. The homology modelling process was performed using the Molecular Operating Environment package, version 2013.10 (Chemical Computing Group, http://www.chemcomp.com). Ten independent intermediate models were built by permutational selection of various loop candidates and side-chain rotamers. The intermediate model that scored best according to the GB/VI scoring function was chosen as the final model (Labute, 2008).

ACKNOWLEDGEMENTS

This work received support from the National Science Foundation of China (91125028) and the Strategic Priority Research Program of the Chinese Academy of Sciences (XDB15030202). We thank Guangzhe Yang (Institute of Soil Science, Chinese Academy of Sciences) for valuable discussion.

SUPPORTING INFORMATION

Additional Supporting Information may be found in the online version of this article.

Figure S1. Representative tail currents for ZmK2.1, ZmK2.1–Δ1, KAT1 and KAT1–Δ1 at pH 7.4 and pH 5.4.

Figure S2. The S3–S4 linker partly contributes to the pH sensitivity of ZmK2.1 and KAT1.

Figure S3. Effects of point mutations to C208 and C211 in the background of ZmK2.1–ΔQ + E92D.

REFERENCES

Berman, H.M., Westbrook, J., Feng, Z., Gilliland, G., Bhat, T., Weissig, H., Shindyalov, I.N. and Bourne, P.E. (2000) The protein data bank. *Nucleic Acids Res.*, **28**, 235–242.

Coulter, K.L., Redeke, C.M. and Vanderberg, C.A. (1995) Identification and molecular localization of a pH-sensing domain for the inward rectifier potassium channel HIR. *Neuron*, **15**, 1157–1168.

Gonzalez, W., Riedelsberger, J., Morales-Navarro, S.E., Caballero, J., Alzate-Morales, J.H., Gonzalez-Nilo, F.D. and Dreyer, I. (2012) The pH sensor of the plant K^+ uptake channel KAT1 is built from a sensory cloud rather than from single key amino acids. *Biochem. J.* **442**, 57–63.

Hoth, S. and Hedrich, R. (1999) Distinct molecular bases for pH sensitivity of the guard cell K^+ channels KST1 and KAT1. *J. Biol. Chem.* **274**, 11599–11603.

Hoth, S., Dreyer, I., Dietrich, P., Becker, D., Müller-Röber, B. and Hedrich, R. (1997) Molecular basis of plant-specific acid activation of K^+ uptake channels. *Proc. Natl Acad. Sci. USA*, **94**, 4806–4810.

Hoth, S., Geiger, D., Becker, D. and Hedrich, R. (2001) The pore of plant K^+ channels is involved in voltage and pH sensing: domain-swapping between different K^+ channel α–subunits. *Plant Cell*, **13**, 943–952.

Jiang, Y., Lee, A., Chen, J., Ruta, V., Cadene, M., Chait, B.T. and MacKinnon, R. (2003) X–ray structure of a voltage-dependent K^+ channel. *Nature*, **423**, 33–41.

Labute, P. (2008) The generalized Born/volume integral implicit solvent model: estimation of the free energy of hydration using London dispersion instead of atomic surface area. *J. Comp. Chem.*, **29**, 1693–1698.

Lebaudy, A., Vavasseur, A., Hosy, E., Dreyer, I., Leonhardt, N., Thibaud, J.–B., Véry, A.–A., Simonneau, T. and Sentenac, H. (2008) Plant adaptation to fluctuating environment and biomass production are strongly dependent on guard cell potassium channels. *Proc. Natl Acad. Sci. USA*, **105**, 5271–5276.

Li, L., Liu, K., Hu, Y., Li, D. and Luan, S. (2008) Single mutations convert an outward K^+ channel into an inward K^+ channel. *Proc. Natl Acad. Sci. USA*, **105**, 2871–2876.

Müller-Röber, B., Ellenberg, J., Provart, N., Willmitzer, L., Busch, H., Becker, D., Dietrich, P., Hoth, S. and Hedrich, R. (1995) Cloning and electrophysiological analysis of KST1, an inward rectifying K^+ channel expressed in potato guard cells. *EMBO J.* **14**, 2409–2416.

Philippar, K., Buchsenschutz, K., Abshagen, M., Fuchs, I., Geiger, D., Lacombe, B. and Hedrich, R. (2003) The K^+ channel KZM1 mediates potassium uptake into the phloem and guard cells of the C–4 grass *Zea mays*. *J. Biol. Chem.* **278**, 16973–16981.

Pilot, G., Lacombe, B.T., Gaymard, F., Chérel, I., Boucherez, J., Thibaud, J.-B. and Sentenac, H. (2001) Guard cell inward K^+ channel activity in Arabidopsis involves expression of the twin channel subunits KAT1 and KAT2. *J. Biol. Chem.* **276**, 3215–3221.

Pratelli, R., Lacombe, B.T., Torregrosa, L., Gaymard, F., Romieu, C., Thibaud, J.–B. and Sentenac, H. (2002) A grapevine gene encoding a guard cell K^+ channel displays developmental regulation in the grapevine berry. *Plant Physiol.* **128**, 564–577.

Roelfsema, M.R.G. and Hedrich, R. (2005) In the light of stomatal opening: new insights into 'the Watergate'. *New Phytol.* **167**, 665–691.

Schroeder, J.I., Allen, G.J., Hugouvieux, V., Kwak, J.M. and Waner, D. (2001) Guard cell signal transduction. *Annu. Rev. Plant Biol.* **52**, 627–658.

Steidl, J.V. and Yool, A.J. (1999) Differential sensitivity of voltage-gated potassium channels Kv1.5 and Kv1.2 to acidic pH and molecular identification of pH sensor. *Mol. Pharmacol.* **55**, 812–820.

Su, Y.–H., North, H., Grignon, C., Thibaud, J.–B., Sentenac, H. and Véry, A.–A. (2005) Regulation by external K^+ in a maize inward Shaker channel targets transport activity in the high concentration range. *Plant Cell*, **17**, 1532–1548.

Tang, X.D., Marten, I., Dietrich, P., Ivashikina, N., Hedrich, R. and Hoshi, T. (2000) Histidine 118 in the S2–S3 linker specifically controls activation of the KAT1 channel expressed in *Xenopus* oocytes. *Biophys. J.* **78**, 1255–1269.

Thompson, A.N., Posson, D.J., Parsa, P.V. and Nimigean, C.M. (2008) Molecular mechanism of pH sensing in KcsA potassium channels. *Proc. Natl Acad. Sci. USA*, **105**, 6900–6905.

Véry, A.A. and Sentenac, H. (2003) Molecular mechanisms and regulation of K^+ transport in higher plants. *Annu. Rev. Plant Biol.* **54**, 575–603.

Véry, A.A., Gaymard, F., Bosseux, C., Sentenac, H. and Thibaud, J.B. (1995) Expression of a cloned plant K^+ channel in *Xenopus* oocytes: analysis of macroscopic currents. *Plant J.* **7**, 321–332.

Véry, A.-A., Nieves-Cordones, M., Daly, M., Khan, I., Fizames, C. and Sentenac, H. (2014) Molecular biology of K^+ transport across the plant cell membrane: what do we learn from comparison between plant species? *J. Plant Physiol.* **171**, 748–769.

Yang, G., Sentenac, H., Very, A.-A. and Su, Y. (2015) Complex interactions among residues within pore region determine the K^+ dependence of a KAT1-type potassium channel AmKAT1. *Plant J.* **83**, 401–412.

Yon, J. and Fried, M. (1989) Precise gene fusion by PCR. *Nucleic Acids Res.* **17**, 4895.

Zhang, Y.D., Véry, A.A., Wang, L.M., Deng, Y.W., Sentenac, H. and Huang, D.F. (2011) A K^+ channel from salt-tolerant melon inhibited by Na^+. *New Phytol.* **189**, 856–868.

© 2016 The Authors
The Plant Journal © 2016 John Wiley & Sons Ltd,